High Energy Physics and Nuclear Physics

Volume 15, Number 3

A Study of the Basic Characteristics of Proportional Inclined Chamber

Wang Jianchun, Ma Wengan, Xu Zizong, Chen Hongfang and Lin Zhirong

Modern Physics Department, University of Science and Technology of China, Hefei, Anhui, China

A detailed study of the basic characteristics of the proportional inclined chamber is conducted by analyzing the data from both beam test and theoretical simulation of the chamber. It shows that the position accuracy in the wire plane along the direction perpendicular to anode wires is better than 200 μm and the theoretical simulation can explain the experimental results very well.

1. INTRODUCTION

Combined with electromagnetic calorimeter, the Proportional Inclined Chamber (PIC) can be used as a luminosity monitor and tagging system of two-photon process events on a large electron-positron collider spectrometer. This system is mounted in the forward and backward small angle regions of the spectrometer. In order to obtain good accuracy of both luminosity measurement and the transverse momentum measurement of a two-photo process event, it needs a good spatial resolution for high energy incident electrons with accuracy better than 0.2 mm in wire-plane along the direction perpendicular to anode wires [1]. An ordinary drift chamber can also provide good spacial resolution, but its counting rate is much lower than that of a proportional wire chamber. The anode-wire-plane of PIC is inclined towards the average direction of the incident tracks. We define α as the angle between the normal line of PIC anode-wire-plane and the direction of the incident charged particle. When α increases, the number N of wires fired by the incident particle will also increase. Because each track provides N data of time, the spatial resolution of PIC is much better than that of an ordinary wire chamber. In the first order approximation, the measurement of the impact point on anode-wire-plane is independent of drift velocity. Bettini *et al.* [2] showed that PIC can provide spatial resolution of about 100 μm, two-track resolution of about 300 μm, and that the resolution angle of the track direction can reach 1°.

Received on November 15, 1990.

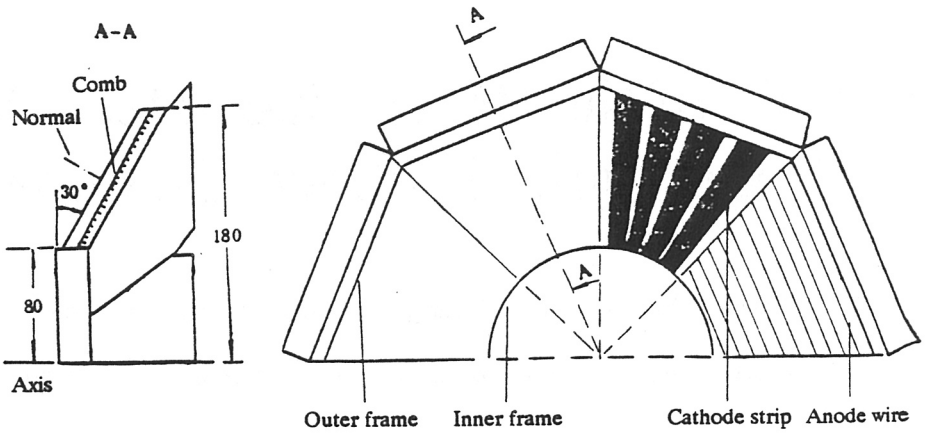

Fig. 1
A sketch of PIC structure.

We will report the results from both the beam test and the theoretical simulation of PIC. They are well fitted with each other, and the specifications of the chamber have met our requirements.

2. DESCRIPTION OF THE PIC STRUCTURE

Fig. 1 shows a sketch of PIC. It is the frustum of a octagonal pyramid. At each edge, there is a upstanding supporting comb. The combs are precisely-processed 1-mm-thick epoxy resin plates. The 0.3-mm-wide, 1-mm-deep notches are located on the top of the comb. The space between notches is 2.12 ± 0.02 mm. The anode wires are fixed in notches one by one, and the wire spacing s is 2 mm. The anode wire is gold-plated tungsten filament which is 20 μm in diameter. The distance between the anode-wire-plane and cathode plane is 8 mm. The angle between the normal line of pyramid side plane and the axis of pyramid is 30°. The incident high energy electron, parallel to the axis of the pyramid, forms a track in the chamber sensitive region, covering a range of about 5 wires. We can deduce the radial coordinate ρ of the track impact point on wire-plane from the measured drift time on certain wires. Each of the sectors of the PIC cathode plane is divided into 16 radial cathode strips with equal angle intervals. The width of each strip varies from 3 mm to 8 mm along the radial direction. The measurement of the position of the center of charge induced on cathode strips can provide the information on the coordinate ϕ, which is the azimuth angle of incident particle passing through the wire plane [3].

The working cathode voltage of PIC is –4.4 kV, and the electric potential on the anode wires are kept at zero. The Ar(80%) + CO_2(20%) mixed gas is used as working gas under 1 atom. The gas is radiation-resistant, safe and cost-effective.

3. SIMULATION AND CALCULATION OF DRIFT VELOCITY AND ELECTRIC FIELD STRENGTH

We used WIRCHA package [4] to evaluate drift velocity and electric field strength.

3.1 Calculation of Drift Velocity of Electrons [5]

The drift velocity of electrons is not proportional to E/p (where E is the electric field strength, and p is the pressure of the gas in the chamber), unlike that of ion. Even in a very low electric field, the mobility of electrons is not yet a constant. So we used drift velocity rather than mobility to describe the drift characteristic of electrons. Assuming that the mean time period between two collisions of an electron is τ and that the mean drift velocity is $\bar{w} = (eE/2m)\tau$, where e and m are the charge and mass of electron, respectively. τ is dependent on the energy of electron gas pressure and the gas components. In order to determine τ, we first need to calculate the energy distribution of electrons. The relation between energy distribution and electric field strength is

$$F(\varepsilon) = C\sqrt{\varepsilon}\ \exp\left\{-\int \frac{3\varepsilon\Lambda(\varepsilon)\mathrm{d}\varepsilon}{[eE\lambda(\varepsilon)]^2 + 3\varepsilon k T\Lambda(\varepsilon)}\right\},$$

where C is a constant. ε the energy of electrons. k the Boltzmann constant, T the working temperature of the chamber gas, $\Lambda(\varepsilon)$ the average energy loss factor per collision, and $\lambda(\varepsilon)$ the average free path. Denoting P_i as the content of each part of the gas mixture, we have

$$\Lambda(\varepsilon) = \sum_i P_i\Lambda_i(\varepsilon).$$

Based on this knowledge, we learn that in electric field with electric field strength E, the drift velocity and diffusivity of electrons are

$$W(E) = -\frac{2}{3}\frac{eE}{m}\int \varepsilon\lambda(\varepsilon)\frac{\partial[F(\varepsilon)v^{-1}]}{\partial\varepsilon}\,\mathrm{d}\varepsilon;$$

$$D(E) = \frac{1}{3}\int v\lambda(\varepsilon)F(\varepsilon)\mathrm{d}\varepsilon,$$

where v is the velocity of electrons with energy ε.

3.2 Evaluation of Electric Field Strength in the Chamber

We used the method of periodically arranged wire chambers provided by the WIRCHA program to calculate electric field strength in the chamber. The main idea of this method is as follows [4,6]. Assuming that there is a very big wire chamber and the distance between its two cathode plates is very large, we place in the position of each anode wire a small wire chamber with the same size as what we want to study. Then we use the wires with the same radius and infinite lengths to substitute for the frame and cathode plates of all small chambers. So every small chamber can be described by parameters of position, radius and electric potential of a set of wires. Again, each corresponding wire of each small chamber and the two cathodes of a big chamber form another wire chamber. We can calculate the electric potential in all those chambers. Finally, the superposition of

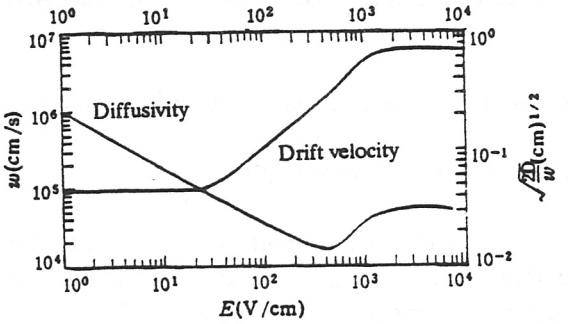

Fig. 2
Correlation among drift velocity, diffusivity and electric field strength.

all these potentials contributed by single large chambers describes the distribution of electric field in the small chamber.

Usually, electric potential formula in multi-wire chamber is [7-9]:

$$V(x, y) \simeq \frac{V_0}{\frac{2\pi L}{s} - 2\ln\frac{2\pi R_0}{s}} \left\{ \left(\frac{2\pi L}{s}\right) - \ln\left[4\left(\sin^2\frac{\pi(x-x_0)}{s} + \sinh^2\frac{\pi(y-y_0)}{s}\right)\right]\right\}.$$

which satisfies the condition $L >> s$, where x_0 and y_0 are the coordinates of the anode wire nearest to the origin point, R_0 the radius of anode wire and V_0 the applied electric potential on the anode wire.

3.3 Correlation Between Drift Velocity, Diffusivity and Electric Field Strength

Using the formula in Section 3.1, we obtain the correlation between drift velocity, diffusivity and electric field strength as shown in Fig. 2. The gas mixture is Ar(80%) + CO_2(20%) and working pressure is 1 atm. In Fig. 2, the diffusivity is defined as $\sqrt{\frac{2D}{W}}$ in $cm^{1/2}$. Fig. 2 shows that when electric field strength is greater than 2×10^3 V/cm, the drift velocity and diffusivity become constants. The spatial position of the track is calculated on the basis of drift-time data and drift velocity. So constant drift velocity and diffusivity are needed in order to obtain good resolution. Moreover, drift velocity and diffusivity ought to be in such condition that they are less affected by the instablity of anode potential. So we choose chamber working voltage as −4.4 kV. In this condition, calculation results show that the strength is greater than 4×10^3 V/cm almost everywhere in the chamber. So drift velocity is about 60 μm/ns, which is in the region with a stable value.

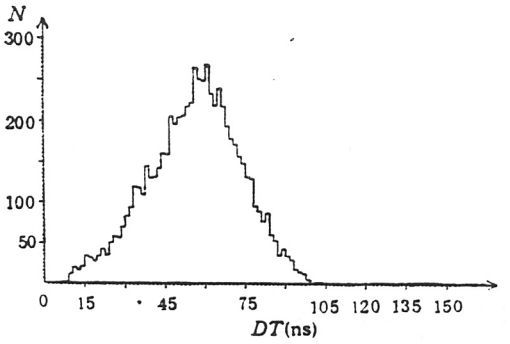

Fig. 3
The distribution of the drift time difference DT obtained from the beam test.

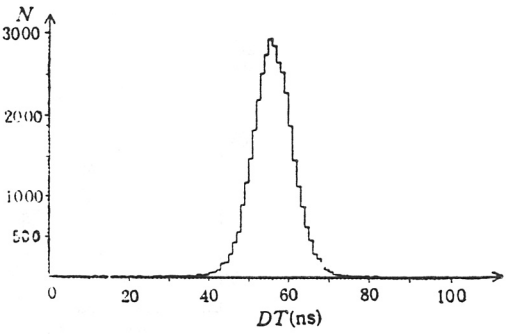

Fig. 4
The distribution of the drift time difference DT obtained from the Monte-Carlo simulation.

4. STUDY OF BASIC CHARACTERISTIC OF PIC

Beam test of PIC is done on beam line X3 at SPS CERN. The components of beam particles are minimum ionization particles (e, μ, π of energy from 10 GeV to 50 GeV). The angle between the normal line of wire plane and the beam direction is 30° ± 1°. When cathode voltage is –4.4 kV, most incident particles will fire 5 sense wires. The arriving time T_i^m related to the reference signal (trigger signal) of the ith wire's signal is the data obtained from the beam test.

In order to further understand the characteristic of PIC, we use the distribution of calculated electric field and drift velocity, diffusivity to obtain isochronous lines and generate minimum ionization particles and corresponding primary clusters. Then we can obtain the minimum drift time T_i^s of all clusters according to isochronous lines established before.

We now analyze the data T_i^s from the simulation and T_i^m from the beam test and compare the two.

4.1 Drift Velocity w and Spatial Resolution Error σ_x

When the angle between the normal of PIC wire plane and the track of minimum ionization particle is a constant, and if we ignore the curvature of the field lines in the neighborhood of the sense anode wire, there must exist a linear correlation between the drift time and the position of corresponding wire. So the difference $DT = |T_i - T_{i+1}|$ between drift times of two contiguous wires will satisfy $DT = |T_i - T_{i+1}| = s/(w \cdot \mathrm{tg}\alpha)$, where s is the spacing of anode wires. When α is 30°, most tracks fire 5 wires. So in the data analyzation, we select 5-wire-fired events. In evaluating DT to each wire, we abandon the DT data on the wire corresponding to the smallest drift time (there the curvature of the field line breaks the above linear correlation). Thus we obtain the distribution of DT from both the beam test and the simulation as shows in Fig. 3 and Fig. 4, respectively, with α = 30°, s = 2 mm. From Fig. 3, we know that for beam test the mean value of DT is $<DT>$ = 56.0 ns and σ_{DT} = 17.1 ns. The estimated drift velocity is $w = s/(<DT>\mathrm{tg}\alpha)$ = 61.9 μm/ns. Fig. 4 shows that $<DT>$ = 55.9 ns, σ_{DT} = 5.2 ns and the drift velocity w = 62.0 μm/ns.

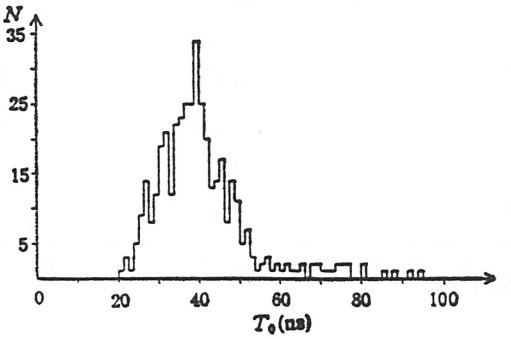

Fig. 5
The distribution of the passage time T obtained from beam test.

The error of the impact point coordinate x on the wire plane can be estimated from σ_{DT}, i.e., the standard deviation of the DT distribution. This is a quantity related to the resolution in the drift time measurement. The error on time measurement is $\varepsilon_T = \sigma_{DT}/\sqrt{2}$. When each track fires N wires, the one-dimensional position error is

$$\sigma_x = \varepsilon_T \cdot w \cdot \mathrm{tg}\,\alpha/\sqrt{N} = \sigma_{DT} \cdot w \cdot \mathrm{tg}\,\alpha/\sqrt{2N}.$$

When $N = 5$, we have $\sigma_x = 193\ \mu$m from the beam test and $\sigma_x = 53\ \mu$m from the simulation.

A difference between σ_{DT} obtained from the beam test and from the simulation is that the values of σ_{DT} obtained from the beam test include the deviation caused by incident angle error ($\alpha = 30° \pm 1°$), while in the simulation we take $\alpha = 30°$ with no error. Moreover, the amplitude fluctuation of output signal causes time swing in the electronic timing system.

4.2 The Passage Time T_0

Drift time calculated from Monte-Carlo simulation does not include electric time delay, so in the simulation $T_0 = 0$. But in the beam test, things are different. We assume that the electric time delay of all wires are the same, as denoted by T_0. To determine T_0 we can look at the distribution of the shortest measured drift time for tracks passing a sense wire. We select tracks passing as near as possible to a wire by requiring the measured drift time on the left neighboring wire to be equal to that on the right neighboring wire. In fact, we select events that satisfy condition $|\Delta T| \leq 6$ ns (a clock period), where ΔT is the drift time difference between that measured on the left and right neighboring wires. So we can obtain more events, and the track goes still very near to the sense wire. From the measured drift time of this wire we obtain the time distribution as shown in Fig. 5. This figure shows that the peak of the distribution curve is at the position of 40 ns, and the half height width is about 7 ns. We will use T_0 as passage time to obtain the real drift time T_i in the following sections.

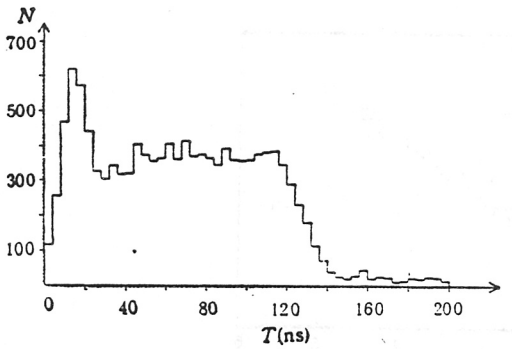

Fig. 6
The drift time distribution obtained from the beam test.

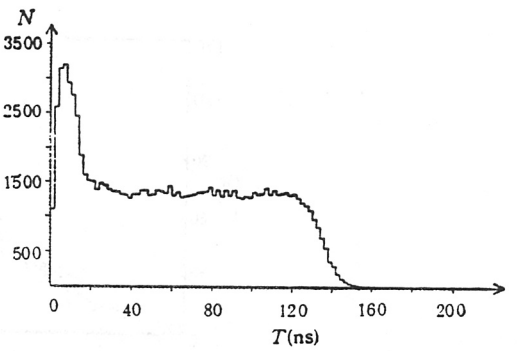

Fig. 7
The drift time distribution obtained from the Monte-Carlo simulation.

4.3 Drift Time Spectrum

On the basis of the beam test drift time data T_i^m, we obtain the real drift time $T_i = T_i^m - T_0$. The distribution of T_i is shown in Fig. 6. In Monte-Carlo simulation, we choose the angle between the normal of PIC wire plane and tracks as 30° and the average ionization free path $\bar{\lambda}$ = 300 μm. We simulate ion clusters along the track and obtain the shortest drift time of each wire as the measured time from these clusters. The drift time spectrum from simulation is shown in Fig. 7.

Comparing Fig. 6 with Fig. 7, we can see that the simulation result fits well with that from the beam test and there is a peak at about $T \approx 8$ ns. When T is greater than 16 ns, the distribution curve moves to a flat region. The flat region exists between 20 ns and 130 ns. After 130 ns, the flat curve becomes a "tail" (see Figs. 6 and 7). Here we can give a simple explanation [5]. The incident particle beam is a uniform one. In the region near anode wire, the electric field strength is much greater than that in the uniform region and there exists the curvature of the field lines. The number of incident particles per drift line length in unit time is greater than that in the uniform region. So a peak is shown in both Fig. 6 and Fig. 7. In the uniform region, which is far away from anode wire, the number of incident particles per drift line length in unit time keeps constant. So in the spectrum there is a flat region. In the region between these two, the electric field strength declines from high value to low one, showing a gradient between peak and flat regions. After the flat region there is a "tail" because the gap between anode plane and cathode plane is finite. The drift distance of electrons from cathode to anode wire is not the same, therefore it makes statistical fluctuations in drift time. From the above analysis, we can estimate the drift velocity from drift time spectrum. Choosing average maximum drift time as 128 ns, we obtain the drift velocity w = 8 mm/ 128 ns = 62.5 μm/ns. It is roughly the same as the above result.

4.4 Correlation of Drift Time and Impact Point Position

PIC is used as a detector to position particle tracks. If one can determine both the impact point position of incident particle on anode plane and the track direction, space position of track is

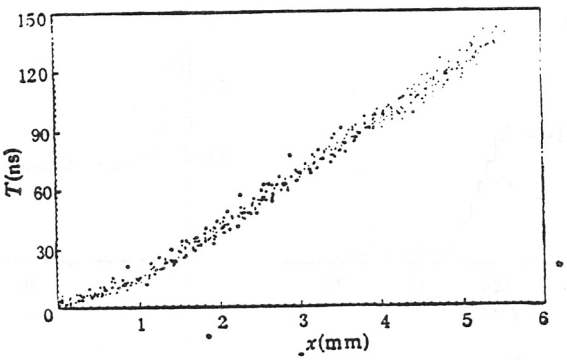

Fig. 8
The correlation between drift time and space position from Monte-Carlo simulation.

determined. In 2-dimensional space, it is easy to determine the track direction by using the formula $\mathrm{ctg}\alpha = w \cdot DT/s$. The position of impact point can be determined through the space-time correlation.

With the incident wide beam at a constant angle, the drift time measured on every anode sense wire has a correlation with the distance from the wire to the impact point. Fig. 8 shows this correlation obtained by Monte-Carlo simulation. In Fig. 8, when the distance is large enough, the distribution satisfies the linear correlation. Because the track passes the uniform region of the wire, where the electric lines are almost parallel, the dots from the T-x simulation distribute approximately as a straight line (x is the distance between the impact point on the wire plane and fired wire). When x is short enough, the track passes through the high strength region where the electric line is curved and where the linear correlation between T and x vanishes. According to Fig. 8, we fitted a linear correlation of T-x for $x > 1.0$ mm, and obtained $t = 28.04x - 15.4$, i.e., $x \doteq 0.0357t + 0.55$, where x is in mm and t in ns. We can obtain the approximate drift velocity as $w = 0.0357 \times \sqrt{3}$. It is also roughly the same with the result obtained before.

5. CONCLUSION

We studied the basic characteristics of PIC from both experiment and Monte-Carlo simulation. The results show that the drift velocity of electrons under the working condition is about 62 μm/ns. The passage time of the drift time measured on anode wire is 40 ns. It is also shown that PIC can be used as luminosity monitor in large electron-positron collider with its 1-dimension spatial resolution better than 200 μm.

Computer simulation is also successful. The distribution of drift time and space-time correlation are fitted with the result of the from experiment.

ACKNOWLEDGMENT

We would like to express our gratitude to our colleagues at CERN and to Professor Samuel C. C. Ting for his help in the course of the PIC beam test.

REFERENCES

[1] Technical Proposal, L3, May 1983.
[2] Bettini A. *et al.*, *Nucl. Instrum. Methods*, 204(1), (1982) 65.
[3] Xu Zizong *et al.*, *Nuclear Electronics & Detection Technology*, **10** (1990) 153.
[4] Fehlmann J. *et al.*, WIRCHA-A Program Package to Simulate Drift Chamber, ETH. TEC DETECTOR GROUP, Internal Report, 1983.
[5] Tang Xiaowei *et al.*, Experimental Methods of Particle Physics, People's Education Press, (1982) 35.
[6] Ma Wengan *et al.*, *Journal of China University of Science & Technology*, *19* (1989) 131.
[7] Buchholz H., Electrische and Magnetische Potentialfelder, Spring, Berlin. 1957. p. 90.
[8] Erskine G. A., *Nucl. Instrum. Methods*, **105** (1972) 565.
[9] Morse P. M. and Feshbach H., Methods of Theoretical Physics, McGraw-Hill, New York, 1953, p. 489.